Surfactant-Aided Hydrothermal Synthesis and Carbon Dioxide Adsorption Behavior of Three-Dimensionally Mesoporous Calcium Oxide Single-Crystallites with Tri-, Tetra-, and Hexagonal Morphologies

Caixin Liu, Lei Zhang, Jiguang Deng, Qing Mu, Hongxing Dai,* and Hong He

Laboratory of Catalysis Chemistry and Nanoscience, Department of Chemistry and Chemical Engineering, Beijing University of Technology, Beijing 100124, P.R. China

Received: July 22, 2008; Revised Manuscript Received: September 4, 2008

Three-dimensionally (3D) mesoporous single-crystalline CaO nano- and microparticles with tri-, tetra-, and hexagonal morphologies have been successfully fabricated using a surfactant (P123, CTAB, or PEG) assisted hydrothermal dissolution−recrystallization strategy with irregular nonporous CaO powders as the starting material. The as-synthesized calcium oxide samples are characterized by means of techniques such as X-ray diffraction, scanning electron microscopy, high-resolution transmission electron microscopy/selected area electron diffraction, Fourier-transfer infrared spectroscopy, thermogravimetric analysis/differential scanning calorimetry, and N_2 adsorption−desorption. It is shown that the introduction of a surfactant has an important effect on the morphology and pore structure of the synthesized CaO samples. With P123 or PEG as template, a higher hydrothermal temperature and longer hydrothermal time favor the generation of more regular morphological CaO entities with a higher surface area. Among the surfactants adopted in the present work, PEG is the most effective in the fabrication of high-surface-area 3D mesoporous CaO. Under the conditions of hydrothermal temperature of 240 °C and hydrothermal time of 72 h in the presence of PEG and after calcination at 600 °C for 3 h in an oxygen flow, one can obtain a single-crystalline 3D mesoporous CaO material with a surface area of 257 m^2/g. The possible formation mechanism of single-crystalline 3D wormhole-like mesoporous CaO is also discussed. These high-surface-area mesoporous CaO samples exhibit excellent CO_2 adsorption behavior. The highest amount of CO_2 desorbed from the CaO hydrothermally fabricated with PEG at 240 °C for 72 h and calcination at 600 °C for 3 h achieves 770 μmol CO_2/g. It is suggested that the rise in surface area and the formation of 3D wormhole-like mesopores contribute to the enhanced CO_2 adsorption capacity of CaO.

1. Introduction

Alkaline earth oxides have a wide range of applications in microelectronics, adsorption, and catalysis. Due to their unique strong basicity,[1] alkaline earth oxides can be used as adsorbent for acidic gas adsorption,[2−9] catalysts for biodiesel production via the transesterification of triglycerides with alcohol of low molecular weight,[10−13] and catalyst supports for the selective oxidation of light hydrocarbons.[14] Among the alkaline earth oxides, MgO and CaO have been investigated extensively. Calcium oxide is an exceptionally important material suitable for use as catalyst, toxic waste remediation agent, or an additive in refractory and paint.[15] For example, CaO catalyzes the hydrogenation and isomerization of alkenes,[16−18] oxidative coupling of methane[19,20] and oxidative dehydrogenation of ethane,[20] and H_2 (or CH_4)−O_2 exchanges.[21] Another merit of CaO is its strong ability to adsorb SO_2[4,5] and CO_2.[6−9,22] CaO is usually produced by the thermal decomposition of calcium carbonate or nitrate, which gives rise to micro- or nanometer nonporous CaO particles with low surface areas.

Although there are several reports on the fabrication of nanosized CaO[15,23−25] in the literature, the work on the synthesis of three-dimensionally (3D) mesoporous CaO has been rarely seen so far. The only relevant work was done by Sotirchos and Smith,[26] who adopted a calcium-enriched bio-oil decomposition route to generate porous CaO particles with a maximal surface area of 24 m^2/g, and by Sasaoka and co-workers,[27] who obtained macroporous CaO samples with surface areas less than 15 m^2/g using a water−acetic acid swelling method. Recently, Liu et al. synthesized macroporous (pore size = 1−10 μm) CaO with high surface area (139 m^2/g) via a wetness impregnation pathway with active carbon as hard template and calcium nitrate as metal source.[28] In order to generate high-surface-area mesoporous CaO, we recently modified the hydrothermal dissolution−recrystallization method[29] by introducing a surfactant as soft template. Previously, we adopted such a similar method to successfully synthesize 3D wormhole-like mesoporous MgO single-crystallites with high surface areas (near 300 m^2/g).[30] Herein, we report the P123-, CTAB-, and PEG-assisted hydrothermal fabrication and characterization of tri-, tetra-, and hexagonal single-crystalline CaO particles with mesoporous framework. To the best of our knowledge, this is the first report regarding the synthesis of mesoporous CaO using the surfactant-aided hydrothermal strategy.

2. Experimental Section

Single-Crystalline Porous CaO Fabrication. The single-crystalline porous CaO samples were fabricated using the surfactant-assisted hydrothermal dissolution−recrystallization strategy[29,30] with bulk CaO powders as calcium source. The typical synthesis procedure is as follows: 3.45 g of triblock copolymer poly(ethylene glycol)-*block*-poly(propylene glycol)-

* Corresponding author. Tel.: +8610-6739-6588; Fax: +8610-6739-1983; E-mail: hxdai@bjut.edu.cn.

10.1021/jp8064568 CCC: $40.75
Published on Web 11/14/2008

block-poly(ethylene glycol) ($EO_{20}PO_{70}EO_{20}$, P123, $M_{aver.}$ = 5800, Aldrich) or hexadecyltrimethyl ammonium bromide (CTAB, Beijing Chemical Reagent Co., 99.9%) or poly(ethylene glycol) (PEG, $M_{aver.}$ = 1000, Sinopharm Chemcal Reagent Co., 99.5%) was first dissolved in 60 mL of deionized water; then, 1.12 g of CaO powder (Beijing Chemical Plant, 99%) was added to the solution. The molar ratio of CaO to surfactant (P123, CTAB, or PEG) adopted was 1/1.25. After ultrasonic stirring for 24 h, the mixed solution was transferred to a 100 mL Teflon-lined stainless steel autoclave (packed volume = 80 mL), and the autoclave was placed in an oven for hydrothermal processing at a desired temperature (160 or 240 °C) for a desired time (24 or 72 h). The obtained mixture was in turn washed with deionized water (2−3 times) and with ethanol (3−4 times) for the removal of most of the surfactant. After filtration and drying at 80 °C overnight, the substance obtained was the $Ca(OH)_2$ intermediate. After thorough grinding, the powders were heated in an oxygen flow of 80 mL/min at a ramp of 1 °C/min from room temperature (RT) to 600 °C and kept at this temperature for 3 h. The final obtained sample was the single-crystalline porous CaO.

Characterization. X-ray diffraction (XRD) patterns of as-fabricated $Ca(OH)_2$ and CaO samples were recorded on a Bruker/AXS D8 Advance X-ray diffractometer operated at 40 kV and 200 mA using Cu Kα radiation and Ni filter. Crystal phases were identified by referring the diffraction lines to those of the powder diffraction files-1998 ICDD PDF Database. Surface areas, pore size distributions, and N_2 adsorption−desorption isotherms of the samples were measured via N_2 adsorption at −196 °C on an ASAP 2020 (Micromeritics) adsorption analyzer with the samples being outgassed at 250 °C for 2 h under vacuum prior to measurements; surface areas and pore size distributions were calculated according to the Brunauer−Emmett−Teller (BET) and Barrett−Joyner−Halenda (BJH) method, respectively. The images of the samples were recorded by means of scanning electron microscopy (SEM, JEOL JSM 6500F, FEI Quanta 200, and Gemini Zeiss Supra 55) operating at 10 or 20 kV. Before being transferred into the SEM chamber, the sample ultrasound-dispersed in ethanol was allowed to settle and dry on a holder before being introduced to a vacuum evaporator for gold deposition. By means of a JEOL-2010 instrument (operated at 200 kV), high-resolution transmission electron microscopy (HRTEM) images and selected area electron diffraction (SAED) patterns of the samples were obtained. Thermogravimetric analysis (TGA) and differential scanning calorimetric (DSC) analysis were conducted in a nitrogen flow of 100 mL/min at a ramping rate of 10 °C/min on a SDT Q600 instrument (TA).

CO_2 Adsorption Measurement. In order to evaluate the CO_2 adsorption behaviors of the synthesized 3D mesoporous CaO samples, we conducted CO_2 temperature-programmed desorption (CO_2-TPD). The sample was placed in a quartz microreactor (i.d. = 8 mm), and the outlet gases were analyzed online by a mass spectrometer (Hiden HPR20). Before the TPD experiment, 0.1 g of the as-fabricated CaO sample was thermally treated in helium (flow rate = 30 mL/min) at 550 °C for 1 h, followed by cooling in helium to RT (for the removal of adsorbed water). Then, the CaO sample was exposed to a CO_2 (99.99% in purity) flow of 40 mL/min at RT for 1 h, followed by removal of physisorbed CO_2 by means of helium flushing (He flow = 40 mL/min) at RT for 3 h. The desorption of chemisorbed CO_2 took place in the helium flow with the sample being heated from RT to 850 °C at a rate of 10 °C/min. The amount of CO_2 desorbed from the sample was quantified by calibrating the peak area against that of a standard CO_2 pulse (20.0 μL).

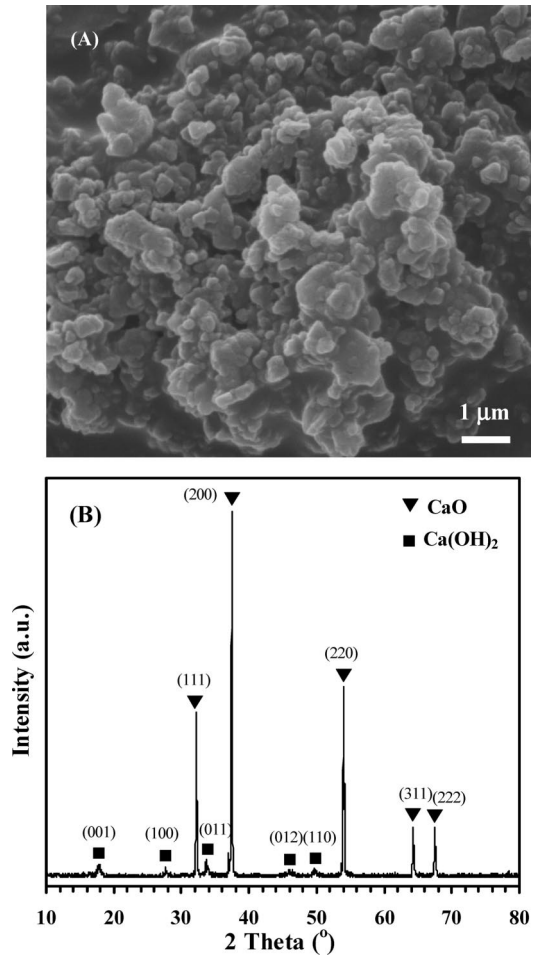

Figure 1. (A) SEM image and (B) XRD pattern of the raw CaO powders employed in the present study.

In order to obtain information on CO_2 adsorption, we treated the fabricated CaO sample (obtained by hydrothermal treatment with P123, CTAB, or PEG at 160 or 240 °C for 72 h and calcination at 600 °C for 3 h) in a He flow of 30 mL/min at 550 °C for 1 h, followed by cooling in the same atmosphere to RT, and then switching to a CO_2 flow of 40 mL/min at RT for 1 h for the adsorption of CO_2. Fourier-transfer infrared spectroscopic (FT-IR) spectra (400 to 4000 cm^{-1} with a resolution of 0.4 cm^{-1}) of the CO_2-adsorbed samples and those after CO_2-TPD experiments, as well as the $Ca(OH)_2$ intermediate and corresponding CaO product synthesized hydrothermally with PEG at 240 °C for 72 h (1 wt % sample + 99 wt % KBr) were recorded on a Bruker Vertex 70 spectrometer.

3. Results and Discussion

Figure 1 shows the SEM image and XRD pattern of the CaO raw material employed in the present study. It is observed that the raw CaO powders were irregular in shape with particle size ranging from 400 to 2000 nm (Figure 1A) and a small amount of $Ca(OH)_2$ existed in the raw material (Figure 1B). The wide-angle and representative small-angle XRD patterns of the fabricated CaO and $Ca(OH)_2$ samples synthesized under different hydrothermal conditions are shown in Figure 2. The XRD peaks (Figures 2A,B(e,f)) of the as-received calcium oxide samples can be indexed to face-centered cubic CaO and those (Figure 2B(g)) of the calcium hydroxide intermediate obtained

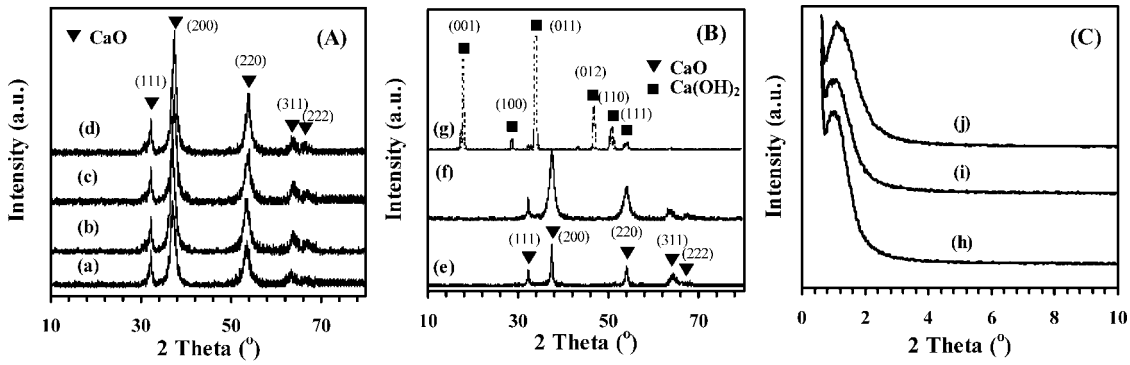

Figure 2. (A) XRD patterns of the CaO samples synthesized by hydrothermal treatment (a) without surfactant, (b) with P123, (c) with CTAB, and (d) with PEG at 160 °C for 24 h and calcined at 600 °C for 3 h; (B) XRD patterns of (e,f) CaO collected after hydrothermal treatment (e) without surfactant, (f) with PEG at 240 °C for 72 h and calcined at 600 °C for 3 h, and of (g) $Ca(OH)_2$ collected after hydrothermal treatment with PEG at 240 °C for 72 h without calcination; and (C) small-angle XRD patterns of CaO collected after hydrothermal treatment with (h) P123 at 240 °C for 72 h, (i) CTAB at 160 °C for 72 h, (j) PEG at 240 °C for 72 h, and calcined at 600 °C for 3 h.

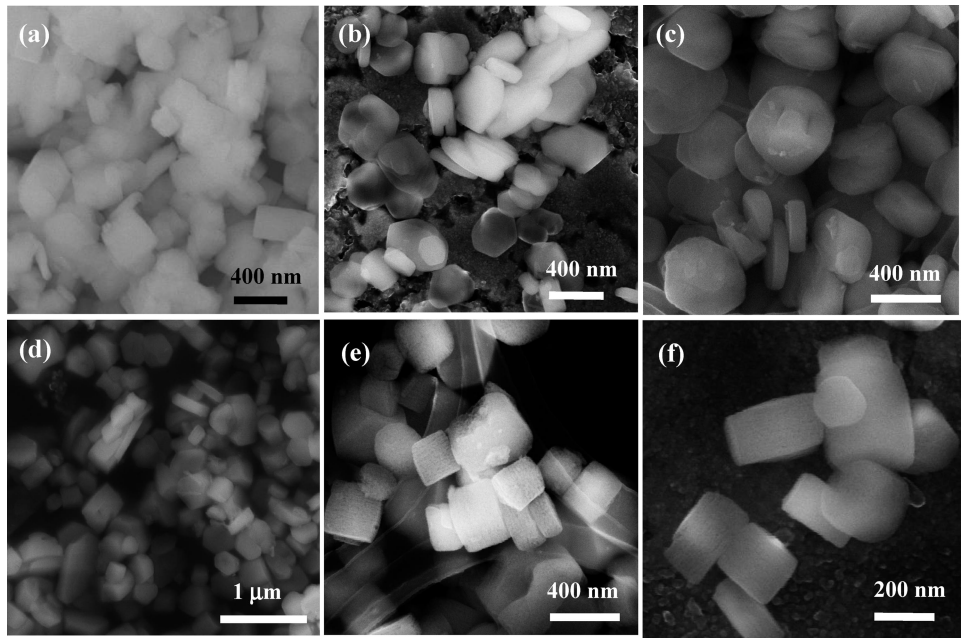

Figure 3. SEM images of the CaO samples synthesized by hydrothermal treatment at 240 °C for 72 h (a) without surfactant, (b) with P123, (c) with CTAB, and (d−f) with PEG, and calcined at 600 °C for 3 h.

after hydrothermal treatment with PEG at 240 °C for 72 h to hexagonal $Ca(OH)_2$; their lattice parameters agree well with the corresponding standard values given in JCPDS PDF# 82−1690 (CaO) and PDF# 84−1274 ($Ca(OH)_2$), respectively. From Figure 2A, one can see that the peak intensities of the CaO samples fabricated with the aid of P123, CTAB, or PEG are rather similar and stronger than those of the CaO sample derived from the surfactant-free hydrothermal process. The CaO sample derived hydrothermally at 240 °C for 72 h without the use of a surfactant and calcined at 600 °C for 3 h shows diffraction peaks (Figure 2B(e)) of weaker intensity in comparison to those (Figures 2B(f)) of the CaO sample derived with the use of PEG at the same hydrothermal temperature for 72 h. The results indicate that the former is inferior to the latter in crystallinity. As observed in Figure 2C, there is a diffraction peak at $2\theta =$ ca. 1°, indicating the presence of mesopores in the three CaO samples; furthermore, the small-angle diffraction peak shifts from $2\theta = 0.9°$ to 1.2° and its intensity varies depending upon the nature of the surfactant adopted. Obviously, the small-angle diffraction peak of CaO after hydrothermal treatment with PEG at 240 °C for 72 h is the highest in intensity, denoting that there is a significant improvement in pore structure. The results suggest that a higher hydrothermal temperature favors the formation of basically ordered mesoporous architecture.

Representative SEM images of the CaO samples fabricated with and without surfactant-assisted hydrothermal treatment at 240 °C for 72 h and calcination at 600 °C for 3 h are shown in Figure 3. It is observed that these CaO samples contain particles with tri-, tetra-, and hexagonal morphologies, among which the surfactant-free derived CaO samples are mainly composed of irregular tetra- and hexagonal particles, the P123-derived ones exhibit tri- and hexagonal morphologies, and the PEG-derived ones dominantly show tetragonal architectures. The nature of surfactant not only exerts an influence on the surface morphology of the as-received CaO samples, but also significantly affects the pore structures and surface areas as confirmed by the BET results. The trigonal CaO particles display a lateral length of 90−220 nm, the hexagonal ones exhibit a thickness of 60−200 nm and a lateral length of 80−400 nm, and the tetragonal ones show a length of 200−750 nm and a width of 50−360 nm.

Figure 4 provides the representative HRTEM images and the corresponding SAED patterns of the CaO samples obtained after hydrothermal treatment under different conditions. One can observe the presence of tri-, hexa-, and

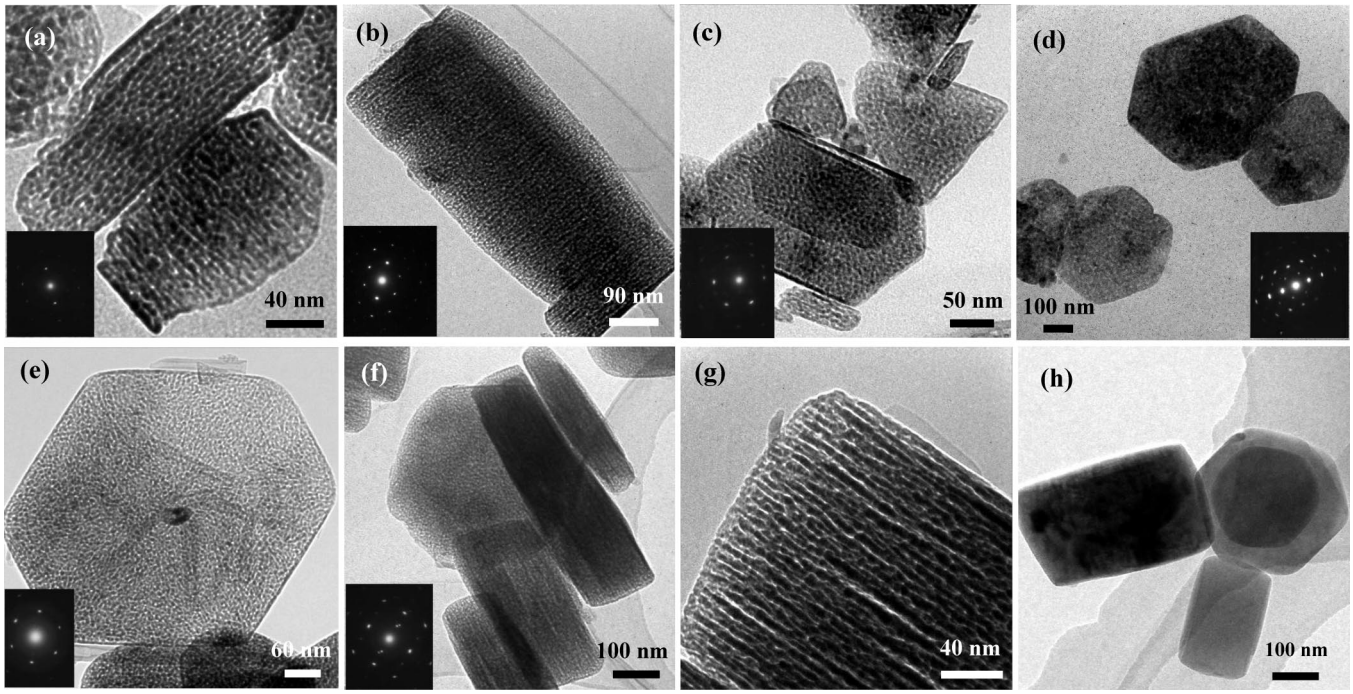

Figure 4. HRTEM images of the CaO samples synthesized by hydrothermal treatment (a) without surfactant at 160 °C for 24 h, (b) without surfactant at 240 °C for 72 h, (c) with P123 at 240 °C for 72 h, and (d) with CTAB at 160 °C for 72 h, (e) with CTAB at 240 °C for 72 h, (f,g) with PEG at 240 °C for 72 h, and calcined at 600 °C for 3 h, as well as of (h) the $Ca(OH)_2$ intermediate synthesized by hydrothermal treatment with PEG at 240 °C for 72 h without calcination. The insets are the corresponding SAED patterns of the CaO samples.

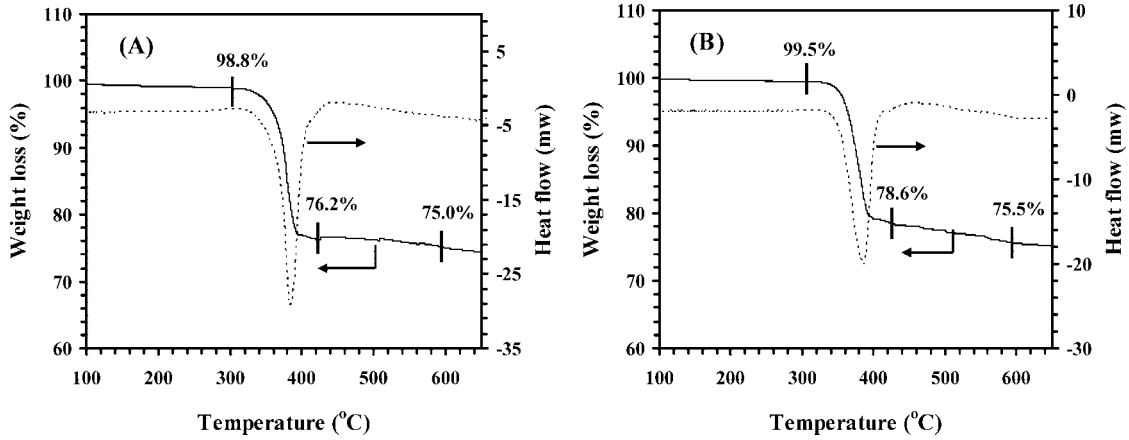

Figure 5. TGA (solid line) and DSC (dashed line) plots of the $Ca(OH)_2$ products synthesized by hydrothermal treatment with (A) P123 at 240 °C for 72 h and (B) PEG at 240 °C for 72 h.

tetragonal CaO particles; the CaO particles with tri- and hexagonal morphologies exhibit disordered 3D wormhole-like mesopores, whereas the tetragonal CaO particles display roughly ordered distorted 3D mesorpores uniformly distributed in the entities, and these mesorpores are monotonously arrayed along the direction parallel to the laterals of tetragonal entities. The dominant morphology of the CaO particles derived from the surfactant-free hydrothermal processing either at 160 °C for 24 h or at 240 °C for 72 h followed by calcination at 600 °C for 3 h is irregular tetragonal, and a higher temperature and longer time of hydrothermal treatment favor the growth of more regular tetragonal CaO entities. In the CaO samples fabricated by P123-templated hydrothermal treatment at 240 °C for 72 h and calcination at 600 °C for 3 h, the particles displayed a feature of tri- and hexagonal architectures. Shown in Figure 4(d,e) are the HRTEM images of the CaO samples synthesized by hydrothermal treatment with CTAB at 160 °C for 72 h or 240 °C for 72 h and calcination at 600 °C for 3 h. As can be seen, the CaO samples mainly contain hexagonal particles with 3D wormhole-like mesopores. It is clear that the CaO particles synthesized by hydrothermal treatment with PEG at 240 °C for 72 h and calcination at 600 °C for 3 h exhibit tetragonal (in majority) and hexagonal (in minority) morphologies, which are much more regular than those derived from the surfactant-free hydrothermal treatments. Furthermore, from the SAED patterns (insets of Figure 4(a−f)), one can observe alignments of bright electron diffraction spots, in which there is a difference in the number of diffraction spots of each sample. It indicates the formation of single-crystalline CaO, and the single-crystallinity is varied from sample to sample.

Shown in Figure 5 are the TGA/DSC profiles of the $Ca(OH)_2$ intermediates obtained via hydrothermal treatment with P123 at 240 °C for 72 h (Figure 5(A)) and with PEG at 240 °C for 72 h (Figure 5(B)). For each of the two calcium hydroxide intermediates, a significant weight loss (22.6% for

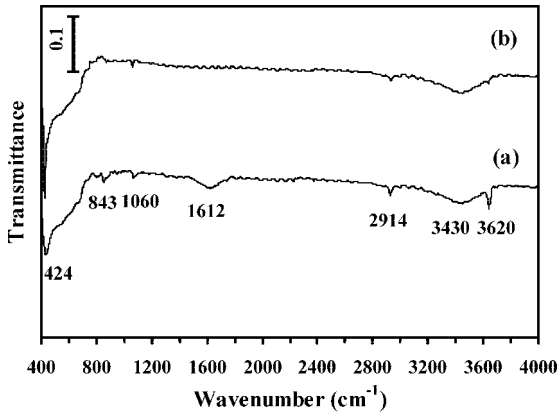

Figure 6. FT-IR spectra of the (a) uncalcined $Ca(OH)_2$ and (b) 600 °C-calcined CaO samples fabricated by hydrothermal treatment with PEG at 240 °C for 72 h.

the $Ca(OH)_2$ sample derived from the P123-aided hydrothermal treatment at 240 °C for 72 h or 20.9% for the $Ca(OH)_2$ sample derived from the PEG-assisted hydrothermal treatment at 240 °C for 72 h) is observed in the temperature range 310−430 °C, together with a well-defined endothermic peak at 384−387 °C. Such a weight loss can be attributed to the thermal decomposition of $Ca(OH)_2$. Tang et al.[23] also detected a similar weight loss (20.4%) in the temperature range 300−500 °C during the decomposition of calcium hydroxide. The observed weight loss (23.8−24.0%) in the range 318−600 °C is slightly smaller than the theoretical value (24.3%) calculated on the assumption of total dehydration of $Ca(OH)_2$ to CaO. The results indicate that nearly complete conversion of $Ca(OH)_2$ to CaO takes place below 600 °C. It implies that the surfactant used in the fabrication of mesoporous CaO samples had been almost totally removed after filtering and washing with deionized water and ethanol. A piece of supporting evidence is from the FT-IR results of the $Ca(OH)_2$ intermediate and CaO samples obtained hydrothermally with PEG at 240 °C for 72 h and calcination at 600 °C for 3 h, as shown in Figure 6. There is a strong IR absorption band at 424 cm^{-1} in the two samples, ascribable to the lattice vibrations of $Ca(OH)_2$ and CaO.[31] The appearance of a rather weak absorption band at 2914 cm^{-1} due to the $-CH_2CH_2$ stretching vibration[32] and a weak absorption at 1060 cm^{-1} due to the C−O stretching vibration[32] of residual surfactant (PEG) molecules on the $Ca(OH)_2$ or CaO surfaces reveals that only a slight amount of the surfactant is retained in the fabricated CaO sample, in good agreement with the results of TGA/DSC investigations (Figure 5). The absorptions at 3430 and 1612 cm^{-1} can be attributed to the stretching and bending vibrations of hydrogen-bonded surface OH groups (adsorbed water),[33] respectively. The sharp band at 3620 cm^{-1} can be ascribed to the stretching vibrations of bulk OH groups of $Ca(OH)_2$.[34] The very weak absorption band at 843 cm^{-1} may be attributed to the crystalline phase of PEG.[35,36] After calcination in an O_2 flow at 600 °C for 3 h, the absorption bands at 843 and 1612 cm^{-1} disappear and the band at 3620 cm^{-1} decreases considerably in intensity, indicating that most of the PEG has been removed and the $Ca(OH)_2$ phase has been almost totally dehydrated to CaO. This result is consistent with the outcome of TGA studies (Figure 5).

Figure 7 shows the N_2 adsorption−desorption isotherms and pore size distributions of the CaO samples fabricated with surfactant-assisted hydrothermal treatments under different conditions as well as that of the $Ca(OH)_2$ intermediate synthesized by the hydrothermal treatment with PEG at 240 °C for 72 h before calcination. It is observed that the isotherm of the $Ca(OH)_2$ intermediate exhibits type III characteristics with a H3 hysteresis loop,[37] which can be related to the formation of slit-shaped pores in the aggregates of platelike particles. The absence of an adsorption isotherm plateau at relative pressure near unity suggests the presence of macropores,[37,38] whereas the appearance of an H1 hysteresis loop in the p/p_0 range 0.4−0.8 denotes the presence of mesopores.[37,39] Apparently, there are macropores in the as-synthesized $Ca(OH)_2$ intermediate (Figure 7A(d)). The appearance of dual hysteresis loops is an indication of the presence of bimodal pores (mesopores and macropores) in each of the three CaO samples (Figure 7A(a−c)). The mesopores are in the tri-, tetra-, and hexagonal CaO entities, as confirmed by the HRTEM images of these samples (Figure 4). As for the macropores, they originate from the aggregates of platelike particles. As shown in Figure 7B, the synthesized CaO after hydrothermal treatment with P123 at 240 °C for 72 h exhibits a relatively wide pore size distribution (Figure 7B(a)) with an average pore diameter of 4.6 nm (Table 1); By changing the surfactant from P123 to CTAB or PEG, the so-obtained CaO material shows a feature of two-peaked pore size distribution with the diameter of 2.4 and 3.3 nm (Figures 7B(b,c)), respectively, and the average pore size of the two samples is accordingly 4.2 and 3.3 nm (Table 1). Such solid materials with 3D wormhole-like meso- and macroporous structure may find use in gas adsorption and heterogeneous catalysis, because they can reduce transport limitations for gas molecules and hence improve the adsorption efficiency and catalytic performance.[40,41]

The textural parameters of the CaO products and $Ca(OH)_2$ intermediate obtained under various synthetic conditions are summarized in Table 1. One can see that all the synthesized CaO samples have much higher surface areas, larger pore volumes, and smaller pore sizes than the raw CaO powders. It is observed that the CaO samples fabricated hydrothermally without surfactant at 160 °C for 24 h and at 240 °C for 72 h and calcined at 600 °C for 3 h possess surface areas (141−160 m^2/g), pore volumes (0.20−0.25 cm^3/g), and average pore diameters (4.2−4.5 nm); the surface areas are much higher than that (24 m^2/g) of the calcium oxide sample obtained from the decomposition of calcium-enriched bio-oil[26] and that (15 m^2/g) of the calcium oxide sample derived from the swelling method.[27] With the introduction of a nonionic surfactant, the surface area of the fabricated CaO sample is enhanced at a higher hydrothermal temperature. The CaO sample synthesized with CTAB at 160 °C for 72 h and calcined at 600 °C for 3 h shows a surface area of 221 m^2/g, a pore volume of 0.28 cm^3/g, and an average pore diameter of 4.2 nm. A further rise in the hydrothermal temperature to 240 °C causes the surface area of the CTAB-derived CaO sample to decrease. The CaO sample synthesized with PEG at 240 °C for 72 h and calcined at 600 °C for 3 h possesses the highest surface area (257 m^2/g); the corresponding pore volume is 0.25 cm^3/g, and the mean pore diameter is 3.3 nm. Compared to the thermally decomposed product, the $Ca(OH)_2$ intermediate exhibits much lower surface area (19 m^2/g), pore volume (0.08 cm^3/g), and larger average pore size (19.1 nm), which reflects the presence of macropores derived from the intraparticle voids. With $Ca(OH)_2$ being dehydrated during calcination, mesopores are generated, resulting in significant enhancement in surface area and pore volume. It should be noted that, in the BET surface area and pore volume

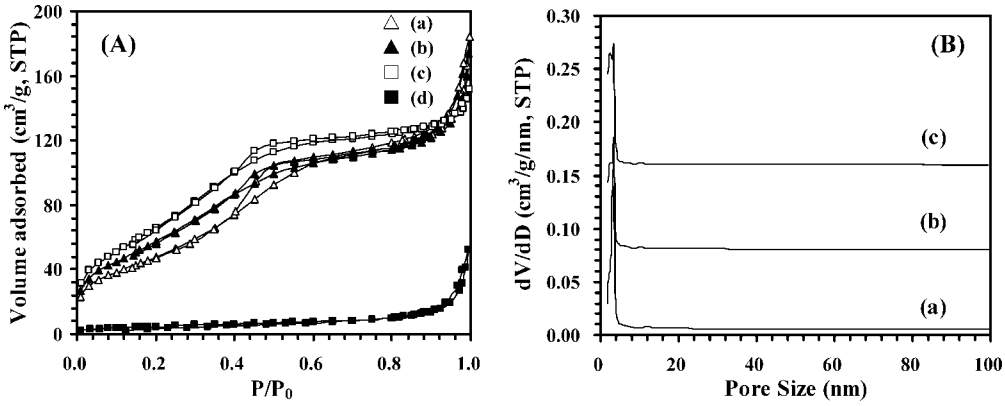

Figure 7. (A) Nitrogen adsorption−desorption isotherms of (a−c) CaO collected after hydrothermal treatment with (a) P123 at 240 °C for 72 h, (b) CTAB at 160 °C for 72 h, (c) PEG at 240 °C for 72 h, and calcined at 600 °C for 3 h, and of (d) $Ca(OH)_2$ collected after hydrothermal treatment with PEG at 240 °C for 72 h without calcination; and (B) pore size distribution curves of the CaO samples.

TABLE 1: Synthetic Conditions and Textural Parameters of the as-Fabricated CaO and $Ca(OH)_2$ Samples

				BET surface area (m^2/g)			pore volume (cm^3/g)			
as-synthesized sample	hydrothermal conditions (°C and h)	calcination conditions (°C and h)	CaO/surfactant molar ratio (mol/mol)	macropore (>40 nm)	mesopore (≤40 nm)	total	macropore (>40 nm)	mesopore (≤40 nm)	total	average pore size (nm)
raw CaO	-	-	-	-	-	9.7	-	-	0.03	10.4
CaO	160 and 24	600 and 3	-	3	138	141	0.04	0.16	0.20	4.2
CaO	240 and 72	600 and 3	-	4	156	160	0.06	0.19	0.25	4.5
CaO	160 and 24	600 and 3	1/1.25 (P123)	2	108	110	0.04	0.15	0.19	4.8
CaO	240 and 72	600 and 3	1/1.25 (P123)	5	176	181	0.08	0.21	0.29	4.6
CaO	160 and 24	600 and 3	1/1.25 (CTAB)	4	175	179	0.07	0.21	0.28	4.5
CaO	160 and 72	600 and 3	1/1.25 (CTAB)	6	215	221	0.08	0.20	0.28	4.2
CaO	240 and 72	600 and 3	1/1.25 (CTAB)	3	174	177	0.04	0.16	0.20	4.2
CaO	160 and 24	600 and 3	1/1.25 (PEG)	5	156	161	0.08	0.20	0.28	5.0
CaO	240 and 72	600 and 3	1/1.25 (PEG)	2	255	257	0.03	0.22	0.25	3.3
$Ca(OH)_2$	240 and 72	-	1/1.25 (PEG)	4	15	19	0.05	0.03	0.08	19.1

of each mesoporous CaO sample, the contribution from the macropores is quite small.

Although the exact formation mechanism of tri-, tetra-, and hexagonal $Ca(OH)_2$ and CaO particles is not clear, the results obtained in the present investigation indicate that the generation of tri-, tetra-, and hexagonal platelike entities is likely to be due to the interaction of the initially formed nanostructured $Ca(OH)_2$ as well as due to the introduced surfactant in the so-called dissolution−recrystallization process.[29] In the past years, a large number of studies have focused on the effects of temperature, concentration, and surfactant composition on the structure (size, morphology, and aggregation number) of surfactant micelles. Among the above listed parameters, temperature has been found to be very crucial. With the rise in temperature, the morphology of the surfactant like P123 changes from spherical to cylindrical, rodlike, wormlike, or even lamellar-shaped.[42−46] Figure 8 illustrates the formation mechanism of mesoporous CaO particles. Under high-temperature hydrothermal conditions, bulk CaO powders are dissolved in water and then hydrolyzed into primary $Ca(OH)_2$ nanoparticles. With the generation of a large amount of primary $Ca(OH)_2$ nanoparticles, these $Ca(OH)_2$ nanoparticles aggregate around the cylindrical, rodlike, wormlike, or lamellar surfactant (P123, CTAB, or PEG) micelles to form the tri-, tetra-, and/or hexagonal-packed domains. It has been accepted that the functional headgroups of the surfactant have coordination bonds or strong interactions with nanoparticles and hence kinetically govern the growth rates of various faces of crystals, thus controlling the morphology.[47−49] It is reasonable to deduce that there is adsorption of surfactant molecules on the well-aligned $Ca(OH)_2$ via hydrogen bonding with the OH groups of Ca^{2+} or via loose coordination with Ca^{2+}; such an interaction between surfactant and $Ca(OH)_2$ would be rather similar to that between P123 and $Mg(OH)_2$ in the synthesis of mesoporous MgO under the P123-aided hydrothermal conditions.[30] Therefore, the above-formed domains could self-assemble layer-by-layer into nano- or microsized $Ca(OH)_2$ platelets of similar morphology. The nonionic polymer PEG has hydrophilic -O- and hydrophobic $-CH_2-CH_2-$ on the long chains. Water is a good solvent for PEG, favoring the full extension of the polymer chains. The O atom of PEG can coordinate with metal ions. The more or less extended order of the polymer chain would provide an environment of organization for metal ions along the polymer backbone. The hydrothermal temperature and time also have an effect on the interaction of PEG polymer chain,[50] thus influencing the morphology of the product. Therefore, the morphologies of the CaO samples synthesized by the PEG-assisted hydrothermal treatment are tetragonal (in majority) and hexagonal (in minority). From the morphologies of the $Ca(OH)_2$ intermediate and the fabricated CaO samples, one can realize that the growth process of the single-crystalline particles is governed by the hydrothermal temperature (which determines the extent of CaO raw material dissolved in water) and surfactant property (which determines the interaction of surfactant and metal ions). A higher temperature as well as a higher pressure favors the dissolution of CaO in water, thus resulting in a morphologically regular $Ca(OH)_2$ and subsequently a product (CaO) with architecture almost the same as that of the $Ca(OH)_2$ intermediate after $Ca(OH)_2$ decomposition. After removal of most of the surfactant via

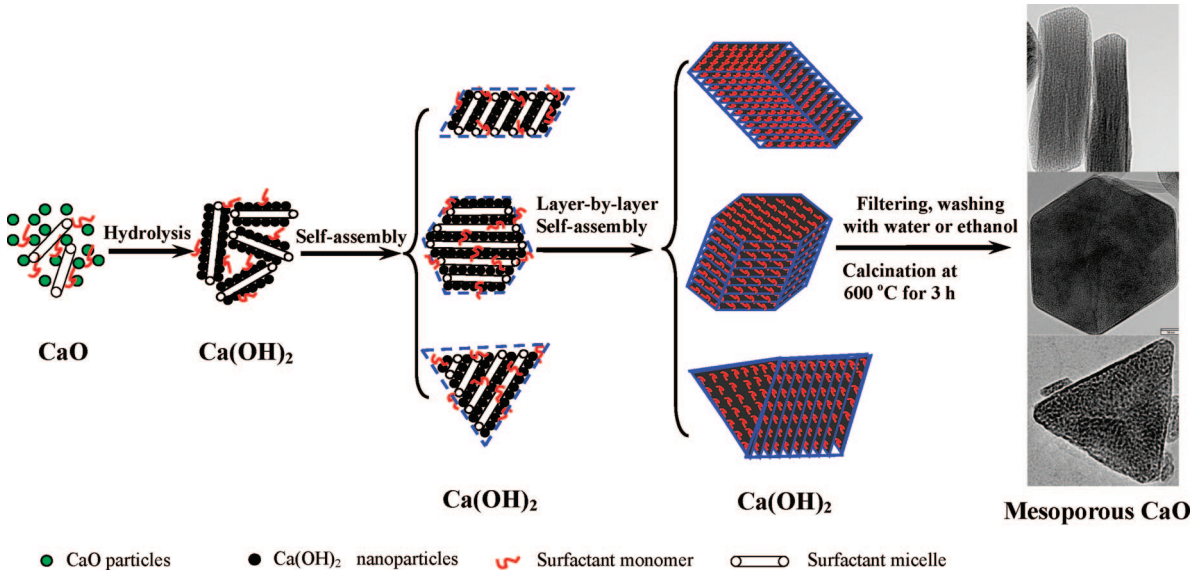

Figure 8. The schematic illustration of formation mechanisms of the $Ca(OH)_2$ intermediates and mesoporous CaO samples under surfactant-assisted hydrothermal and calcination conditions.

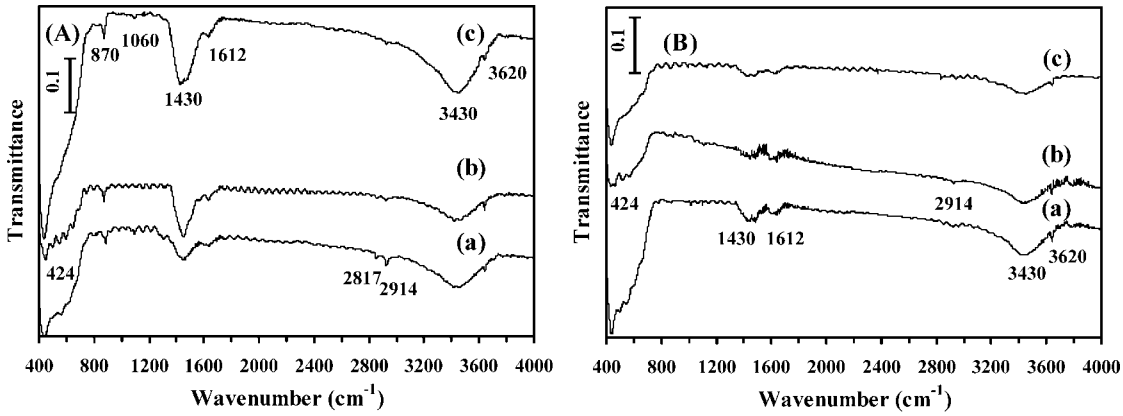

Figure 9. FT-IR spectra of the CaO samples obtained by hydrothermal treatment with (a) P123 at 240 °C for 72 h, (b) CTAB at 160 °C for 72 h, and (c) PEG at 240 °C for 72 h, and calcined at 600 °C for 3 h after (A) exposure to CO_2 at RT for 1 h and (B) CO_2-TPD experiments.

washing with deionized water and ethanol, and calcination at 600 °C for 3 h, the tri-, tetra-, and hexagonal $Ca(OH)_2$ entities change into the corresponding tri-, tetra-, and hexagonally shaped nano- or microscale particles of wormhole-like mesoporous CaO single crystallites. The main morphologies and pore structures of the fabricated CaO particles are determined by the nature of the surfactant adopted as well as the hydrothermal temperature and time.

Shown in Figure 9 are the FT-IR spectra of the CaO samples fabricated by hydrothermal treatment with P123, CTAB, or PEG after CO_2 adsorption at RT and after the CO_2-TPD experiments. In each of the samples, there is a strong IR absorption band at 424 cm^{-1} due to the Ca−O lattice vibration of CaO;[31] two quite weak absorptions at 2817 and 2914 cm^{-1} assignable to the -CH_2CH_2 stretching vibrations, and a weak absorption at 1060 cm^{-1} due to the C−O stretching vibration of surfactant molecules[32] on the mesoporous CaO materials. This implies that the residual surfactant amount is rather low, as confirmed by the TGA results (Figure 5). The presence of adsorbed water is indicated by absorptions at 3430 and 1612 cm^{-1} corresponding to the stretching and bending vibrations of hydrogen-bonded surface OH groups.[33] Due to the easy rehydration of CaO to $Ca(OH)_2$, one can detect a weak and sharp band at 3620 cm^{-1} that can be ascribed to the stretching vibration of bulk OH groups of the hydroxide.[34] The appearance of strong absorption band at 1430 cm^{-1} (due to the symmetric stretching vibration of uni- or bidentate carbonate[8]) and weak absorption band at 870 cm^{-1} demonstrates the presence of carbonate species.[32,51] By comparing the spectra of Figure 9(A) and (B), one can realize that, after the TPD of CO_2, the intensities of absorption bands due to carbonate species as well as water adsorbed on the three CaO samples decrease significantly, indicating that most part of the carbonate adspecies have been desorbed below 700 °C (Figure 10). The temperature (<700 °C) for the desorption of chemisorbed carbonate species from the CaO single crystallites is much lower than that (>800 °C) for the decomposition of calcium carbonate and might be related to the unique 3D mesoporous structure of the former.

Unlike MgO, CaO is a superbase.[1] Therefore, CaO is better than MgO for the adsorption of acidic gases. Figure 10 shows the CO_2-TPD profiles of the CaO samples fabricated by hydrothermal treatment under different conditions. It is observed that there are four desorption peaks, with two peaks in the range 30−300 °C and the other two in the range 500−700 °C. The desorption temperatures are in accordance with those reported by Liu et al.[28] who investigated the desorption of CO_2 from a macroporous CaO (surface area = 139 m^2/g). The amount of desorption corresponding to the two low-temperature and two high-temperature peaks is, respectively, 160 and 410 μmol

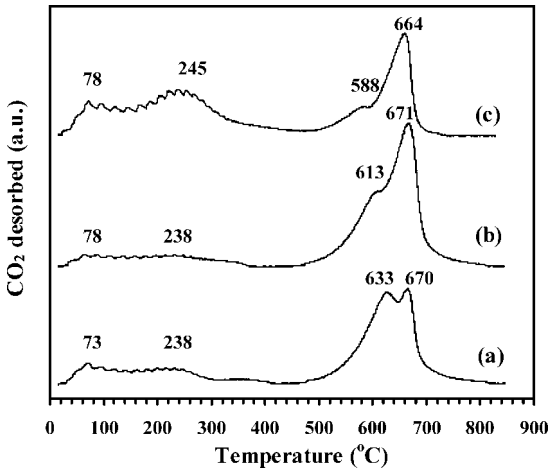

Figure 10. CO_2-TPD profiles of the CaO samples collected after hydrothermal treatment with (a) P123 at 240 °C for 72 h, (b) CTAB at 160 °C for 72 h, and (c) PEG at 240 °C for 72 h, and calcined at 600 °C for 3 h.

CO_2/g over the CaO sample collected after hydrothermal treatment with P123 at 240 °C for 72 h and calcined at 600 °C for 3 h, 220 and 510 μmol CO_2/g over the CaO sample collected after hydrothermal treatment with CTAB at 160 °C for 72 h and calcined at 600 °C for 3 h, and 450 and 320 μmol CO_2/g over the CaO sample collected after hydrothermal treatment with PEG at 240 °C for 72 h and calcined at 600 °C for 3 h. The total desorptions are 570, 730, and 770 μmol CO_2/g, respectively, coinciding with the sequence of the surface area of the three samples. The amounts of CO_2 desorbed from the three mesoporous CaO samples are almost twice as much as the CO_2 uptake (ca. 307 μmol CO_2/g) of the CaO sample (surface area = 30.7 m^2/g)[8] and even nearly an order of magnitude higher than that (54−79 μmol CO_2/g) of the porous CaO sample (surface area = 19 m^2/g) which was sintered at 686 °C for 100 h.[52] Although Liu et al.[28] carried out the CO_2-TPD experiments over the macroporous calcium oxide sample (surface area = 139 m^2/g), they did not give the amount of CO_2 desorbed. From Figure 10, one can also see that the desorption amount of CO_2 adsorbed weakly in the low-temperature range over the PEG-derived CaO sample is much higher than that over the P123- or CTAB-derived CaO sample, but the desorption amount of CO_2 adsorbed strongly in the high-temperature range over the former sample is much lower than those over the latter two samples. This result indicates that the rise in surface area of the CaO sample favors the weak adsorption of CO_2. The presence of 3D wormhole-like mesopores in CaO obtained in the present study may facilitate the adsorption, desorption, and diffusion of CO_2 molecules, partly contributing to the enhanced CO_2 adsorption ability and decreased CO_2 desorption temperature.

4. Conclusions

3D wormhole-like mesoporous nano- and microsized single-crystalline CaO displaying tri-, tetra-, and hexagonal morphologies can be fabricated via the P123, CTAB, or PEG-assisted hydrothermal dissolution−recrystallization pathway. With the introduction of the surfactant at a higher hydrothermal temperature (for nonionic surfactants) and longer hydrothermal time, one can generate a mesoporous CaO material with more regular morphology and higher surface area after calcination of the obtained $Ca(OH)_2$ intermediate. The 3D wormhole-like mesoporous CaO single-crystalline entities fabricated hydrothermally with PEG at 240 °C for 72 h and calcination at 600 °C for 3 h display tetragonal (in majority) and hexagonal (in minority) architectures and possess the highest surface area of 257 m^2/g. These mesoporous CaO materials exhibit an unusually large capacity for CO_2 adsorption, which might be associated with their unique 3D wormhole-like mesoporous structures and high surface areas. The highest amount of CO_2 desorption reaches 770 μmol CO_2/g over the CaO sample hydrothermally generated with PEG at 240 °C for 72 h and calcination at 600 °C for 3 h. The superbasicity and 3D pore structure of such CaO single-crystallites are useful in gas adsorption and catalysis.

Acknowledgment. This work was financially supported by the NSF of China (Grant No. 20473006), the SRF for ROCS (State Education Ministry of China), and the PHR (IHLB) of Beijing Municipality.

References and Notes

(1) Tanabe, K. *Solid Acids and Bases*; Academic Press: New York, 1970.
(2) Renedo, M. J.; González, F.; Pesquera, C.; Ferández, J. *Ind. Eng. Chem. Res.* **2006**, *45*, 3752.
(3) Koper, O. B.; Lagadic, I.; Volodin, A.; Klabunde, K. J. *Chem. Mater.* **1997**, *9*, 2468.
(4) Allal, K. M.; Abbessi, M.; Mansour, A. *Bull. Soc. Chim. Fr.* **1991**, *128*, 880.
(5) Withum, J. A.; Yoon, H. *Environ. Sci. Technol.* **1989**, *23*, 821.
(6) Fukuda, Y.; Tanabe, K. *Bull. Chem. Soc. Jpn.* **1973**, *46*, 1616.
(7) Beruto, D.; Botter, R.; Searcy, A. W. *J. Phys. Chem.* **1984**, *88*, 4052.
(8) Philipp, R.; Fujimoto, K. *J. Phys. Chem.* **1992**, *96*, 9035.
(9) Philipp, R.; Omata, K.; Aoki, A.; Fujimoto, K. *J. Catal.* **1992**, *134*, 422.
(10) Reddy, C. R. V.; Oshel, R.; Verkade, J. G. *Energy Fuels* **2006**, *20*, 1310.
(11) Liu, X.; He, H.; Wang, Y.; Zhu, S.; Piao, X. *Fuel* **2008**, *87*, 216.
(12) Gryglewicz, S. *Bioresour. Technol.* **1999**, *70*, 249.
(13) Watkins, R. S.; Lee, A. F.; Wilson, K. *Green Chem.* **2004**, *6*, 335.
(14) Ji, L.; Liu, J. S. *J. Chem. Soc.: Chem. Commun.* **1996**, 1203.
(15) Olga, B. K.; Isabelle, L.; Alexander, V. *Chem. Mater.* **1997**, *9*, 2468.
(16) Schächter, Y.; Pines, H. *J. Catal.* **1968**, *11*, 147.
(17) Albeck, M.; Rav-Acha, Ch.; Gil-Av, E.; Schächter, O. *J. Catal.* **1971**, *22*, 219.
(18) Hattori, H.; Satoh, A. *J. Catal.* **1976**, *45*, 32.
(19) Carreiro, J. A. S. P.; Baerns, M. *J. Catal.* **1989**, *117*, 258.
(20) Yu, L.; Li, W. Z.; Ducarme, V.; Mirodatos, C.; Martin, G. A. *Appl. Catal. A* **1998**, *175*, 173.
(21) Matsuda, T.; Sugimoto, M.; Yoshiara, H. *Bull. Chem. Soc. Jpn.* **1991**, *64*, 552.
(22) Reddy, E. P.; Smirniotis, P. G. *J. Phys. Chem. B* **2004**, *108*, 7794.
(23) Tang, Z.-X.; Claveau, D.; Corcuff, R.; Belkacemi, K.; Arul, J. *Mater. Lett.* **2008**, *62*, 2096.
(24) Bellobono, I. R.; Selli, E.; Righetto, L. *Mater. Chem. Phys.* **1988**, *19*, 131.
(25) Bellobono, I. R.; Castellano, L.; Tozzi, A. *Mater. Chem. Phys.* **1991**, *28*, 69.
(26) Sotirchos, S. V.; Smith, A. R. *Ind. Eng. Chem. Res.* **2004**, *43*, 1340.
(27) Wu, S.; Uddin, Md. A.; Sasaoka, E. *Energy Fuels* **2005**, *19*, 864.
(28) Liu, S.; Huang, S.; Li, J.; Zhao, N.; Wei, W.; Sun, Y. *Petrochem. Technol. (in Chinese)* **2007**, *36*, 1250.
(29) Yu, J. C.; Xu, A.; Zhang, L.; Song, R.; Wu, L. *J. Phys. Chem. B* **2004**, *108*, 64.
(30) Wang, G. Z.; Zhang, L.; Dai, H. X.; Deng, J. G.; Liu, C. X.; He, H.; Au, C. T. *Inorg. Chem.* **2008**, *47*, 4015.
(31) McDevitt, N. T.; Baun, W. L. *Spectrochim. Acta* **1964**, *20*, 799.
(32) Thierry, B.; Zimmer, L.; McNiven, S.; Finnie, K.; Barbé, C.; Griesser, H. J. *Langmuir*, **2008**, *24*, 8143.
(33) Gadsden, J. A. *Infrared Spectra of Minerals and Related Inorganic Compounds*; Butterworths: London, UK, 1975.
(34) Echterhoff, R.; Hoffmann, P.; Knözinger, E. *Proceedings of the 9th International Congress on Catalysis*; Calgary, 1988; p 1418.
(35) Liu, K. L.; Goh, S. H.; Li, J. *Polymer* **2008**, *49*, 732.
(36) Bailey, J. L.; Koleske, J. V. *Poly(ethylene oxide)*; Academic Press: New York, 1976.
(37) Gregg, S. J.; Sing, K. S. W. *Adsorption, Surface Area and Porosity*, 2nd ed.; Academic Press: London, UK, 1982.
(38) Li, W. C.; Lu, A. H.; Weidenthaler, C.; Schüth, F. *Chem. Mater.* **2004**, *16*, 5676.

(39) Gou, L.; Murphy, C. J. *J. Mater. Chem.* **2004**, *14*, 735.
(40) Sinha, A. K.; Seelan, S.; Tsubota, S.; Haruta, M. *Angew. Chem., Int. Ed.* **2004**, *43*, 1546.
(41) Zhai, S.; Zheng, J.; Shi, X.; Zhang, Y.; Dai, L.; Shan, Y.; He, M.; Wu, D.; Sun, Y. *Catal. Today* **2004**, *93*−*95*, 675.
(42) Alexandridis, P.; Hatton, T. A. *Colloids Surf. A: Physicochem. Eng. Asp.* **1995**, *96*, 1.
(43) Hamley, I. Micellization in PEO-based block copolymers. In *Block copolymers in solution: fundamentals and applications*; John Wiley and Sons, Ltd: Chichester, UK, 2005.
(44) Alexandridis, P.; Holzwarth, J. F.; Hatton, T. A. *Macromolecules* **1994**, *27*, 2414.
(45) Nagarajan, R. *Colloids Surf. B: Biointerfaces* **1999**, *16*, 55.
(46) Lehner, D.; Lindner, H.; Glatter, O. *Langmuir* **2000**, *16*, 1689.
(47) Li, Z. Q.; Xiong, Y. J.; Xie, Y. *Inorg. Chem.* **2003**, *42*, 8105.
(48) Huang, H. H.; Ni, X. P.; Loy, G. L.; Chew, C. H.; Tan, K. L.; Loh, F. C.; Deng, J. F.; Xu, G. Q. *Langmuir* **1996**, *12*, 909.
(49) Sun, Y. G.; Xia, Y. N. *Adv. Mater.* **2002**, *14*, 833.
(50) Shi, X.; Li, M.; Yang, H.; Chen, S.; Yuan, L.; Zhang, K.; Sun, J. *Mater. Res. Bull.* **2007**, *42*, 1649.
(51) Busca, G.; Lorenzelli, V. *Mater. Chem.* **1982**, *7*, 89.
(52) Beruto, D.; Botter, R.; Seary, A. W. *J. Phys. Chem.* **1984**, *88*, 4052.

JP8064568